



Significant promotion of reducing treatment on Pd/TS-1 zeolite for formaldehyde catalytic purification at ambient temperature

Zhaoying Di ^{a,1}, Hongxia Chen ^{a,b,1}, Runduo Zhang ^{a,*}, Hao Wang ^a, Jingbo Jia ^a, Ying Wei ^a

^a State Key Laboratory of Chemical Resource Engineering, Beijing Key Laboratory of Energy Environmental Catalysis, Beijing University of Chemical Technology, Beijing 100029, PR China

^b College of Environmental Engineering, Henan University of Technology, Zhengzhou, Henan 450001, PR China



ARTICLE INFO

Keywords:
TS-1 zeolite
Supported Pd catalysts
Pretreatment
Catalytic oxidation
Formaldehyde

ABSTRACT

This study was conducted to investigate the effect of reducing pretreatment on physicochemical properties of zeolite catalysts and their performances on formaldehyde (HCHO) oxidation at ambient temperature. Pd/TS-1 (Fresh) was tailored by different reductive gases (H₂, CO) and liquid agents [ascorbic acid (AA), ethylene glycol (EG), sodium borohydride (NaBH₄)]. Based on the characterization of HRTEM and CO chemisorption, it was shown that the reducing treatment could significantly reduce the size of Pd nanoparticles (NPs) based on the good dispersion of noble metal. The smallest size of Pd nanoparticles with 5.1 nm was achieved by using NaBH₄ as reducing agent. Accordingly, the best activity was observed on the Pd/TS-1(NaBH₄) sample, pretreated by NaBH₄ in aqueous solution, which could eliminate HCHO completely even at room temperature. Combined with Raman, H₂-TPR, and CO-DRIFT, the excellent catalytic performance of Pd/TS-1(NaBH₄) are mainly ascribed to the high Pd dispersion, superior redox properties and abundant active O₂ species.

1. Introduction

As one of the major indoor air pollutants, formaldehyde (HCHO) is commonly released from furniture, paint, and plywood. It can cause serious health problems such as headache, pneumonia, and eye irritation and is defined as a group I carcinogen by the World Health Organization. Variety of purification methods has been adopted for HCHO abatement such as physical or chemical adsorption, plasma decomposition, biological degradation, and photo/thermo catalytic oxidation [1, 2]. Among them, catalytic oxidation at room temperature is an ideal and effective method for indoor HCHO abatement, which avoids frequent adsorbents regeneration, secondary pollution, and high cost of equipment [3,4]. At present, supported noble-metal (Pd, Pt, Au) [5–7] and transition-metal (Mn, Ce, Co) oxide catalysts [8–10] were literature reported for HCHO elimination. In general, the supported noble-metal catalysts showed better performances for HCHO purification at relatively low temperatures because of their excellent ability to activate oxygen and water molecules. However, limited resource and high price of these noble metals restrict the practical application. Therefore, it is urgent to well utilize these noble metals involved to cut down the catalyst cost by a strategy of high dispersion of active components even

up to an atomic level.

Titanium silicalite-1 (TS-1) has the MFI structure and readily transferred the TiO₂ phase to single Ti atoms in the lattice by isomorphic substitution. It is reported that TS-1 exhibits excellent catalytic activity in many important oxidation reactions [11]. Ti-containing supports (especially TiO₂) have been found to be effective to catalyze the HCHO oxidation [12]. Besides, TS-1 zeolite has good hydrophobicity, which can facilitate desorption of water during the HCHO oxidation process [13]. Additionally, the isomorphic substitution of Si atoms with Ti ones in silicalite skeleton enhanced the oxygen activation ability, which is beneficial for the removal of formaldehyde.

In our previous work, we have prepared the Pd@TS-1 catalyst with Pd loading of 0.2 wt% via an encapsulation strategy by zeolite framework, showing outstanding HCHO removal efficiency along with highly dispersed copper species. Nevertheless, the preparation procedure of Pd@TS-1 catalyst involves relatively complicated manipulation and additional cost of organic encapsulating agent, which limits the corresponding scale-up synthesis aiming to industrial application [14]. As a continuation, this work therefore focuses on exploring a simple method to effectively promote the activity of precious metal catalysts prepared by usual impregnation method through pretreatment.

* Corresponding author.

E-mail address: zhangrd@mail.buct.edu.cn (R. Zhang).

¹ Z. Di and H. Chen contribute equally as the first author.

As we know, two major pretreatment methods including reducing treatment (e.g. by H_2) and oxidizing treatment (e.g. by air or O_2) were reported in the previous literature [15]. Tailoring under the diverse atmospheres, the microstructure and catalytic activity of catalysts (noble metals and supports) will be simultaneously modified. For example, Liu et al. investigated the effects of pretreatment under different atmospheres (H_2 , N_2 , He and Air) on $Pd/\gamma-Al_2O_3$ catalysts for benzene degradation, and found the catalyst pretreated in inert atmospheres was beneficial for enhancing catalytic activity due to the transformation of crystal structure of PdO from the well-defined crystalline phase to the amorphous one along with high concentration of oxygen vacancies [16]. In addition, Lamber et al. announced pretreating of the Pd/SiO_2 sample in H_2 atmosphere may lead to strong metal-support interaction and growth of palladium silicide (Pd_2Si) with respect to the Pd matrix [7]. Chen et al. proposed that the Au/SiO_2 and $Au/ZSM-5$ samples pretreated in H_2 got better activity than those in air, which was attributed to the high Au dispersion and small particle size [17]. However, Chen et al. investigated the effect of O_2 pretreatment on $Ag/MCM-41$ at different temperatures (from 500 °C to 800 °C) for $HCHO$ oxidation, and found that the better catalytic activity was also achieved on the sample pretreated in O_2 stream at 700 °C due to the formation of metallic silver particles with smaller size than those of other samples [18].

The common reduction method is essentially thermal treatment with a gas-phase reduction. However, the operations involving high-temperature reduction are often consuming energy and causing the sintering. Besides, the choice of support has some requirements, because this kind of process needs thermal resistance. Thereafter, it is suggested to use liquid-phase reduction as an alternative method to control the chemical state of noble metals stably. For example, Chen et al. compared the distinct activities on $HCHO$ combustion over catalysts activated by two kinds of reduction (gaseous H_2 or aqueous $HCHO$) for $Pt/ZSM-5$ ($Si/Al=350$) [19]. The results showed that the conversion of $HCHO$ was more than 95%, and the stability was over 100 h at 30 °C, which is attributed to the high ratio of Pd^0 and the excellent adsorption capacity of $HCHO$ on $Pt/ZSM-5(HCHO)$ catalyst. At present, there are various reducing agents used in the liquid-phase reduction including the common sodium borohydride ($NaBH_4$), ethylene glycol [$(CH_2OH)_2$], hydrazine (N_2H_4), ascorbic acid ($C_6H_8O_6$).

In previous reports [15–19], researchers mostly investigated the factor of valence state of active centers during the diverse treatment. In this work, we comprehensively compare all pretreatment methods to explore which method has a better $HCHO$ elimination. And the effects of different reduction-treatment methods on active component particle size, metal dispersibility, redox properties, oxygen species and reaction mechanism are systematically investigated to explore an effective way to improve catalytic activity by tailoring the catalyst structure. The $Pd/TS-1$ sample was prepared and thereafter pretreated with reductive processes including H_2 , CO in gas phase or ascorbic acid, ethylene glycol, sodium borohydride in liquid phase. Meanwhile, the corresponding influences on catalyst properties and catalytic activity for $HCHO$ oxidation are investigated. And physicochemical characterizations including X-ray diffraction (XRD), high-resolution transmission electron microscopy (HRTEM), CO chemisorption, temperature-programmed reduction by hydrogen (H_2 -TPR), Raman, and X-ray photoelectron spectroscopy (XPS) were conducted as well as reaction mechanism for $HCHO$ catalytic oxidation was proposed based on diffuse reflectance infrared Fourier transform spectroscopy (DRIFTS) to disclose the relationship between material structure and catalytic performance. In addition, theoretical calculations are used to calculate the oxygen adsorption capacity of the samples. It is further confirmed that the reduced samples are beneficial for oxygen adsorption and further activation.

2. Experimental

2.1. Catalyst preparation

2.1.1. Gas-phase reduction treatment

$TS-1$ was purchased from Nankai Catalysts Company. And the Si/Ti molar ratio in $TS-1$ is 50. The $TS-1$ supported Pd nanoparticles were synthesized through an incipient wetness impregnation method. For a typical synthesis process, 1 g of $TS-1$ support was immersed into 1.89 mL of 0.01 mol/L $PdCl_2$ solution (0.1 vol% HCl). Then, the mixture was stirred at room temperature for 6 h. Afterwards, the obtained solid was dried in an oven at 80 °C for 12 h, and finally calcined in air atmosphere with a ramp rate of 2 °C/min and held at 450 °C for 4 h. The as-prepared catalysts were denoted as $Pd/TS-1(Fresh)$. The theoretical Pd loading was measured with inductively coupled plasma atomic emission spectrometer (ICP-AES) and the value was close to 0.2 wt%. Finally, the sample was pretreated in different reductive atmospheres (5 vol% H_2 /He or CO/He) at 300 °C, and marked as $Pd/TS-1(H_2)$ or $Pd/TS-1(CO)$, respectively.

2.1.2. Liquid-phase reduction treatment

For comparison, liquid-phase reduction methods with mild condition were adopted during $Pd/TS-1$ preparation using different reductants, including sodium borohydride ($NaBH_4$), ethylene glycol (EG), and ascorbic acid (AA). In this synthesis process, 1 g of $TS-1$ support was firstly dispersed in a mixture of 1.89 mL of 0.01 mol/L $PdCl_2$ solution and 50 mL of deionized water under stirring for 30 min. Afterwards, pre-weighted $NaBH_4$ power ($Pd: NaBH_4 = 1:100$) was quickly added to the above mixture under vigorously stirring. After 6 h, the power was collected after centrifugation, and washed with deionized water and ethanol for several times. Finally, the products were obtained by drying at 60 °C without further calcination and denoted as $Pd/TS-1(NaBH_4)$. For $Pd/TS-1(AA)$, the preparing procedure was similar as that of $NaBH_4$, except that the $NaBH_4$ reductant was replaced by 0.2 g of AA and 1 mL of HCl (0.1 mol/L). The preparation of $Pd/TS-1(EG)$ was as follows: 1 g of $TS-1$ was dispersed in 30 mL of EG, and then sonicated for 30 min. Afterwards, the $PdCl_2$ solution was added into the above mixture and dissolved under stirring at 160 °C in an oil bath. After 4 h, the gray sample was collected by centrifugation and dried at 50 °C in a vacuum.

2.2. Characterization

The crystal structure of as-prepared samples was characterized using Bruker D8-Advance instrument equipped with $Cu K\alpha$ radiation ($\lambda = 1.5406 \text{ \AA}$). The specific surface area and pore size distribution of catalysts were obtained by N_2 sorption isotherm on Quantachrome iQ-3 instrument, and calculated via the Brunauer-Emmett-Teller (BET) equation and DFT method, respectively. The size distribution of Pd nanoparticles was counted from the HRTEM images, taking on a transmission electron microscope (JEM-3010). The Fourier transformed infrared (FT-IR) spectra were collected on a Thermo 4670 instrument with MCT detector. The range of spectra was collected from 400 to 4000 cm^{-1} . Raman spectra were recorded by using a Thermo Fischer DXF spectrometer. And the excitation source was 532 nm laser. The composition and valence state of catalysts were taken on a X-ray photoelectron spectroscopy (XPS, Thermo Fisher) with $C 1s$ peak for calibration. The temperature-programmed reduction by H_2 (H_2 -TPR) experiment was carried out on a chemisorption apparatus (Huasi, China) equipped with TCD. Before the H_2 -TPR experiment, 500 mg of the as-prepared catalysts were pretreated with 30 mL/min 18 vol% O_2/Ar at 200 °C for 30 min. Then the samples were purged in N_2 for 30 min to remove excess O_2 . The samples are reduced in a mixed gas containing 5% H_2 in N_2 at a flow rate of 25 mL/min, and heated to 600 °C at a heating rate of 10 °C/min. The dispersion of Pd was examined by CO pulse chemisorption and performed on the same instrument as that of H_2 -TPR. The specific experimental procedure was as follows: 100 mg of

the sample was first pretreated at 250 °C for 1 h under He atmosphere (30 mL/min). Pulses of 5% CO/He were injected into a quartz reactor to purge the sample surface after the temperature was cooled to 40 °C. The TCD monitors CO consumption signal until adsorption equilibrium. The dispersion of Pd was calculated according to a CO/Pd stoichiometric ratio of 1. The calculation formula of Pd dispersion is as follows:

$$D(\text{Pd dispersion}) = N_s/N_t \quad (1)$$

where N_s is the amount of Pd on the surface; N_t is the amount of Pd in the entire catalyst.

All of the periodic DFT calculations in this work were carried out utilizing the VASP code. At the level of generalized gradient approximation, the Perdew-Burke-Ernzerhof (PBE) of exchange–collection function was used. The standard projector-augmented-wave (PAW) pseudo-potentials were utilized to describe the core-electron interactions with a kinetic energy cutoff value of 450 eV. The Gamma k-points were used for structure optimizations.

The diffuse reflectance infrared Fourier transform spectroscopy of CO (CO-DRIFTS) experiment was carried out on a spectrometer (Thermo 4670) equipped with a MCT detector. Before the test, the high-temperature reaction chamber was filled with the powder samples, and then was purged with He stream for 1 h at 200 °C. After cooling to room temperature, the mixture gas (5% CO/He) was exposed to the sample surface until the intensity of CO remained unchanged. All the spectra were recorded at a resolution of 4 cm⁻¹ for 32 scans. The reaction mechanism of HCHO was also studied by *in situ* DRIFTS. Before the measurements, the sample was first pretreated in N₂ at room temperature for 1 h, and then the background spectrum was collected in the flow of N₂. After that, the HCHO flow was introduced into the system. Meanwhile, the spectra were scanned from 1000 to 4000 cm⁻¹ with 32 scans at a resolution of 4 cm⁻¹.

2.3. Activity measurement

The catalytic activities of HCHO oxidation were measured on a fixed-bed quartz reactor using 0.1 g of the as-prepared sample, which was the same as described in our previous work [14]. The reactant mixture was composed of 110 ppm HCHO, 20% O₂, and N₂ at a flow rate of 100 mL/min with 35% relative humidity (RH). Hence, the gas hourly space velocity (GHSV) was corresponded to 60,000 mL/(g×h). HCHO was generated by flowing N₂ through the paraformaldehyde, which was settled in a water bath. The RH was generated by passing N₂ through a water bubbler. Analyses of reactants and products were monitored online through FT-IR spectrometer (Nicolet 460). The bands at 2350 and 2897 cm⁻¹ were attributed to the stretching vibration of HCHO and CO₂, respectively. The catalytic activity was evaluated by HCHO conversion (Eq. (2)).

$$X_{\text{HCHO}}(\%) = \frac{[\text{HCHO}]_{\text{in}} - [\text{HCHO}]_{\text{out}}}{[\text{HCHO}]_{\text{in}}} \quad (2)$$

where [HCHO]_{in} is the initial HCHO concentration and [HCHO]_{out} is the HCHO concentration in the outlet gas.

Kinetic measurements were also carried out on the above reaction equipment. Besides, in order to eliminate internal and external diffusion limitations, it should be controlled the reaction conditions to keep the HCHO conversion below 20%. The turnover frequency (TOF, s⁻¹) was calculated according to the equation below (Eq. (4)).

$$r_{\text{HCHO}} = \frac{[\text{HCHO}]_{\text{in}} X_{\text{HCHO}} V P_{\text{atm}}}{m_{\text{cat}} w_{\text{Pd}} R T} (\text{mols}^{-1} \text{g}_{\text{Pd}}^{-1}) \quad (3)$$

$$\text{TOF} = \frac{r_{\text{HCHO}} M_{\text{Pd}}}{D_{\text{Pd}}} (\text{s}^{-1}) \quad (4)$$

Where m_{cat} is the weight of sample used in the experiment, w_{Pd} is the Pd loading, V is the total flow rate of the feed, D_{Pd} is the dispersion of Pd,

M_{Pd} is the molecular mass of Pd (106.42 g/mol), R is the molar gas constant [8.314 J/(mol×K)], T was the reaction temperature (298.15 K), P_{atm} was the atmospheric pressure (101.325 kPa).

3. Results and discussion

3.1. Crystal structure, BET surface area, and morphology

Fig. S1(a) showed the XRD patterns of Pd/TS-1 pretreated by diverse reduction methods. All samples displayed the well-resolved characteristic peaks of MFI structure in the 2θ range of 8–10° and 23.0–25.0° [20], indicating that the crystal structure of the samples did not change after reduction treatment. Fig. S1(b) showed that there was a complete peak at 24.4° with no splitting, implying that Ti species was successfully introduced into the framework of zeolite [21]. In addition, the characteristic diffraction peaks of Pd⁰ were hardly observed at 2θ = 40.1° and 46.7° [22], likely owing to the essentially low Pd loading (≤ 0.2%) and its high dispersion on the surface of zeolite.

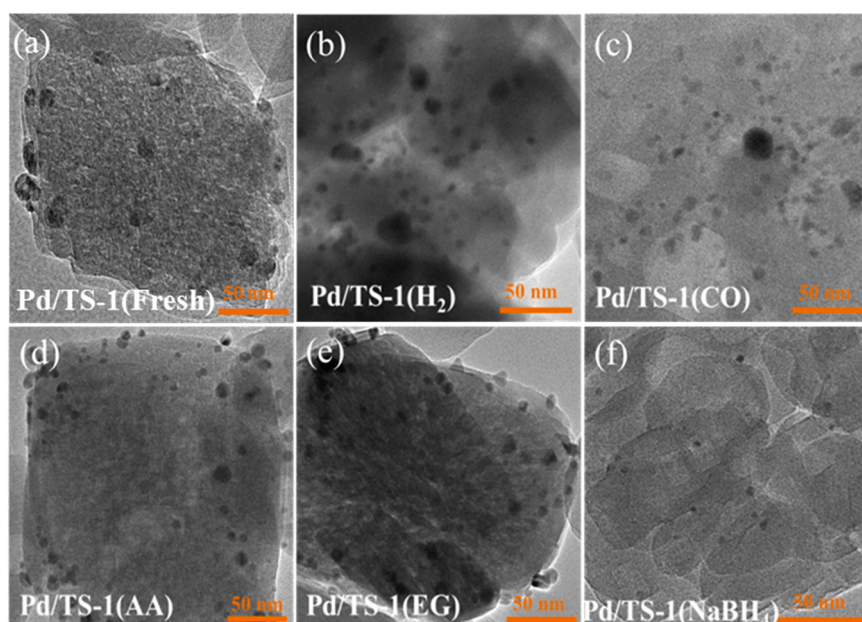
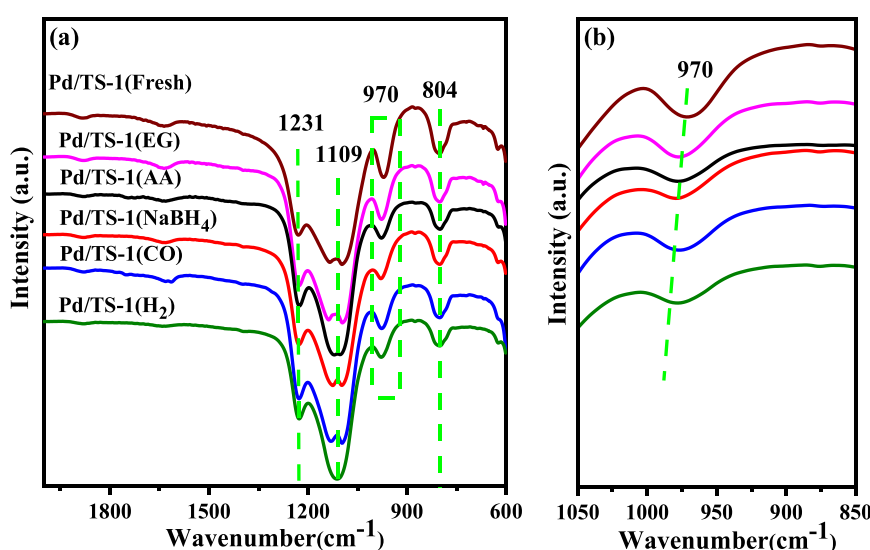
Fig. S2 showed the N₂ sorption isotherms and physical parameters of the as-prepared samples. All of the samples displayed typical IV isotherms with a significant increase at low relative pressure of $P/P_0 < 0.1$, which was suggestive that microporous structure existed [23]. Besides, a H2-shaped hysteresis loop at $P/P_0 = 0.5$ –0.9 was observed, suggesting the presence of mesoporous structure. Fig. S2(b) showed the pore size distribution of the samples obtained by DFT method with ranges of 0.5–1 nm and 2–6 nm, which also confirmed the fact that the micropore and mesopore structure coexisted. In addition, their textural parameters including the BET surface area and pore volume were summarized in Table 1. Obviously, all the samples had similar pore volume, which was around 0.33 cm³/g. However, compared with Pd/TS-1 (Fresh) (459 m²/g), the total BET surface areas of the samples were slightly decreased (around 430 m²/g) after reduction treatment. In order to further explore the reasons for a decline of specific surface area, the external and microporous surface area were calculated using the t-plot method. The external surface areas of all the samples were almost kept unchanged (100 m²/g). However, it could be mainly ascribed to the decrease of microporous surface area from 357 to 312 m²/g. Further heat treatment and micropore blockage during the reduction process may cause this phenomenon.

Furthermore, the morphologies of the samples and particle sizes of Pd were investigated, and the corresponding images were displayed in Fig. 1. All catalysts keep the cubic structure as similar as the TS-1 zeolite with the rough surface. And the particle size of the support was about 300–500 nm. However, the characteristics of active component Pd (dispersion or particle size) exhibited a significant difference as using different methods of reduction. In generally, the size of Pd nanoparticles (12.0 nm) was large when the Pd/TS-1(Fresh) sample was calcined in air by traditional muffle furnace. It is noteworthy that reduction treatment could effectively reduce the size of Pd nanoparticles. For gas-phase reduction, the distribution of Pd nanoparticles was non-uniform on Pd/TS-1(H₂) and Pd/TS-1(CO) due to agglomeration at relatively high temperatures. During the reduction process, the size of Pd nanoparticles increased with the temperature rising because of the Ostwald Ripening behavior. Compared with gaseous treatment, the size of Pd nanoparticles were smaller and more uniform on Pd/TS-1(EG), Pd/TS-1(AA) and Pd/TS-1(NaBH₄) reduced in liquid phase at essentially low or room temperatures. Furthermore, the size distribution of Pd nanoparticles was counted by more than 200 Pd clusters for each catalyst. As shown in Fig. S3, the average size of Pd nanoparticles decreased in the sequence of Pd/TS-1(Fresh) (12.0 nm) > Pd/TS-1(H₂) (9.4 nm) > Pd/TS-1(CO) (9.3 nm) > Pd/TS-1(AA) (8.4 nm) > Pd/TS-1(EG) (7.2 nm) > Pd/TS-1(NaBH₄) (5.1 nm). Apparently, the smallest domain of Pd nanoparticles was achieved on Pd/TS-1(NaBH₄) reduced by NaBH₄. Commonly, Pd nanoparticles with small size can expose more active sites, which is beneficial for the activation of oxygen and the improvement of catalytic activity of formaldehyde oxidation [24].

Table 1

BET surface area, pore volume, Pd content, Pd dispersion, and TOFs.

Sample	$S_{\text{total}}^{\text{a}}$ (m ² /g)	$S_{\text{micro}}^{\text{b}}$ (m ² /g)	$S_{\text{ext}}^{\text{c}}$ (m ² /g)	Pore volume ^d (cm ³ /g)	Pd content ^e (wt%)	Pd dispersion ^f (%)	$\text{TOF} \times 10^{-2}$ (s ⁻¹)
Pd/TS-1(Fresh)	459	357	102	0.32	0.20	11.3	0.04
Pd/TS-1(AA)	433	332	102	0.33	0.19	16.9	0.63
Pd/TS-1(EG)	429	326	103	0.33	0.17	15.8	0.42
Pd/TS-1(NaBH ₄)	430	331	99	0.35	0.18	24.7	2.5
Pd/TS-1(CO)	414	312	102	0.33	0.19	14.7	0.17
Pd/TS-1(H ₂)	429	328	101	0.35	0.20	18.6	1.3

^a S_{total} calculated based on BET method,^b S_{micro} calculated by t-plot method,^c $S_{\text{ext}} = S_{\text{total}} - S_{\text{micro}}$,^d Pore volume calculated by t-plot method,^e Pd content measured using ICP-AES,^f Pd dispersion measured using CO chemisorption.**Fig. 1.** HRTEM images of (a) Pd/TS-1(Fresh), (b) Pd/TS-1(H₂), (c) Pd/TS-1(CO), (d) Pd/TS-1(AA), (e) Pd/TS-1(EG), and (f) Pd/TS-1(NaBH₄).**Fig. 2.** (a) FT-IR patterns of Pd/TS-1 reduced by different methods and (b) Local enlarged drawing of wavenumber at 970 cm⁻¹.

3.2. Elemental coordination on catalyst surface

Fig. 2 shows FT-IR spectra of Pd/TS-1 pretreated by different methods. Four infrared peaks of all the samples at 804, 970, 1109, and 1231 cm^{-1} were detected. The band at 1231 cm^{-1} was attributed to an asymmetrical stretching vibration of MFI framework structure, indicating that the reduction treatment had marginal effect on the structure of zeolite, which is consistent with the results of XRD. The bands at around 804 and 1109 cm^{-1} were assigned to the symmetrical and asymmetrical stretching vibration of $[\text{SiO}_4]$ units, respectively. In addition, the band at 970 cm^{-1} belonged to a vibration of Si-O-Ti in TS-1 [25]. From Fig. 2(b), it could be seen that the intensity of the peak at 970 cm^{-1} of the reduced sample was weakened and shifted to the high wavenumber (981 cm^{-1}), which may be due to the size diminution of Pd nanoparticles and the strong interaction between the tiny Pd cluster and TS-1 support. As for TS-1 zeolite, it is likely to exist unoccupied T sites (metal-vacancy defects in the zeolite) that result in the formation of a local silanol nest [26]. This defect can serve as a site for deposition of noble metal atoms within the zeolite framework [27]. The different reduction pretreatments obtain Pd nanoparticles with diverse sizes, which are confined by the zeolite framework at distinct degrees of defect sites. Thus, the smaller Pd NPs was achieved, the stronger interaction between Pd and TS-1 occurred.

Raman spectra were collected to investigate the surface coordination of Ti species of the samples, and the results are shown in Fig. 3. Four bands at 145, 392, 515 and 640 cm^{-1} were visible. It is generally believed that the bands at 145, 392 and 640 cm^{-1} are attributed to the characteristic vibrations of Ti-O-Ti bond, while the band at 515 cm^{-1} is ascribable to the symmetric stretching vibration of Si-O-Ti bond in TS-1 [28]. Compared with the Pd/TS-1(Fresh) sample, the characteristic peak at 515 cm^{-1} of the reduced samples tended to be wide and low, which possibly due to the enhanced strong interaction between the Pd and TS-1. This phenomenon is in line with the result of Mn doping on TS-1 [29]. It is thus speculated that the strong interaction was due to the extremely small Pd nanoparticles was readily to coordinate with Ti species. These results are in good agreement with those of FT-IR investigation.

3.3. Reducibility, surface element composition, and Pd dispersion

H_2 -TPR experiments are performed to explore the reducibility of the as-prepared sample, which is commonly related to catalytic activity. Bulk PdO_x reduces in hydrogen atmosphere and form Pd NPs, and then

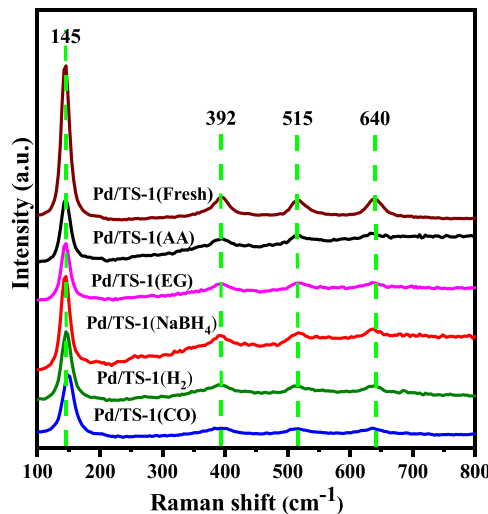


Fig. 3. Raman spectra of Pd/TS-1(Fresh), Pd/TS-1(AA), Pd/TS-1(EG), Pd/TS-1(NaBH_4), Pd/TS-1(H_2), and Pd/TS-1(CO).

hydrogen is adsorbed on the Pd NPs to generate PdH_x [30], which leads to a positive peak at low temperature of the H_2 -TPR file. As the temperature increases, PdH_x decomposes to form hydrogen atoms and Pd NPs. Then the hydrogen atoms move across the surface of Pd NPs to the Pd/TS-1 interface [30,31]. Therefore, negative peaks appear in the H_2 -TPR file.

The profiles are shown in Fig. 4. For the Pd/TS-1(Fresh) sample, there were two reduction peaks at 51 $^{\circ}\text{C}$ and 200 $^{\circ}\text{C}$ respectively, corresponding to the reduction of PdO_x and the generation of PdH_x . Generally, PdO_x was easily reduced to metallic Pd by H_2 at low temperature. Therefore, the peak at 51 $^{\circ}\text{C}$ was attributed to the reduction of PdO_x to Pd, while the negative & flat peak at 200 $^{\circ}\text{C}$ was attributed to the decomposition of PdH_x caused by hydrogen spillover [32]. When Pd/TS-1 was reduced under diverse conditions, the reduction peak of PdO_x was commonly shifted to lower temperatures, with an intense peak at 38 $^{\circ}\text{C}$ observed in the case of Pd/TS-1(NaBH_4). In addition, the negative peak of PdH_x also tends to decompose at relatively lower temperatures (about 60–70 $^{\circ}\text{C}$). Compared with the PdO_x species with large particles on the surface of the Pd/TS-1 (Fresh) sample, the catalysts after reduction treatment have smaller Pd nanoparticles. Among them, the smaller Pd NPs adsorb hydrogen more weakly, which leads to a decrease in the decomposition temperature of PdH_x [33]. It indicates that the reduced catalyst had good low-temperature reducibility, usually associated with better mobility of the corresponding oxygen species. However, there were high-temperature reduction peak at ca. 400 $^{\circ}\text{C}$ on the Pd/TS-1(NaBH_4) and Pd/TS-1(H_2) samples, likely corresponding to some PdO_x nanoparticles, which were difficult to be reduced in H_2 atmosphere. This implied that the PdO_x reduction was easily affected by the size of the metal particles and the characteristics of the support. Generally, it can be considered that there are some highly dispersed PdO_x particles hardly reduced by H_2 due to the strong interaction between the support and the metal nanoparticles [34]. Table S1 shows the hydrogen consumption and release of the Pd/TS-1 samples. Except for the Pd/TS-1 (CO) and Pd/TS-1 (Fresh) samples, the high-temperature hydrogen consumption of the other reduced Pd/TS-1 samples is greater than the low-temperature hydrogen consumption. The strong interaction between PdO_x and the support causes PdO_x to be reduced in the high temperature and requires higher hydrogen consumption.

Surface chemical states of the samples were characterized by the XPS technique, and the Pd 3d XPS of the samples were shown in Fig. 5. The Pd 3d spectra could be deconvoluted into four peaks using the curve-

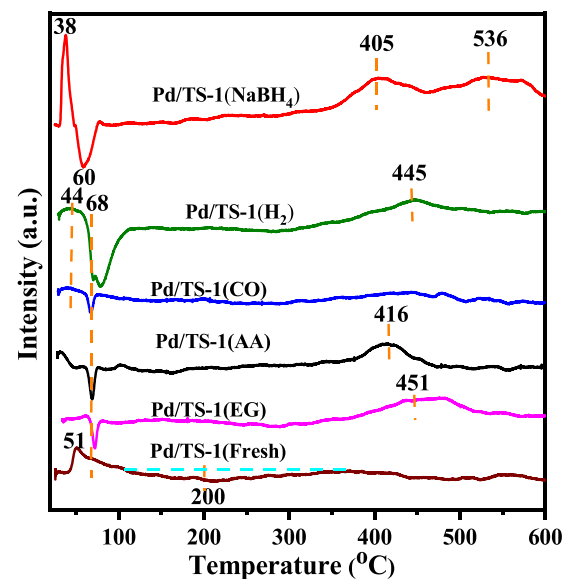


Fig. 4. H_2 -TPR of Pd/TS-1(Fresh), Pd/TS-1(AA), Pd/TS-1(EG), Pd/TS-1(NaBH_4), Pd/TS-1(CO), and Pd/TS-1(H_2).

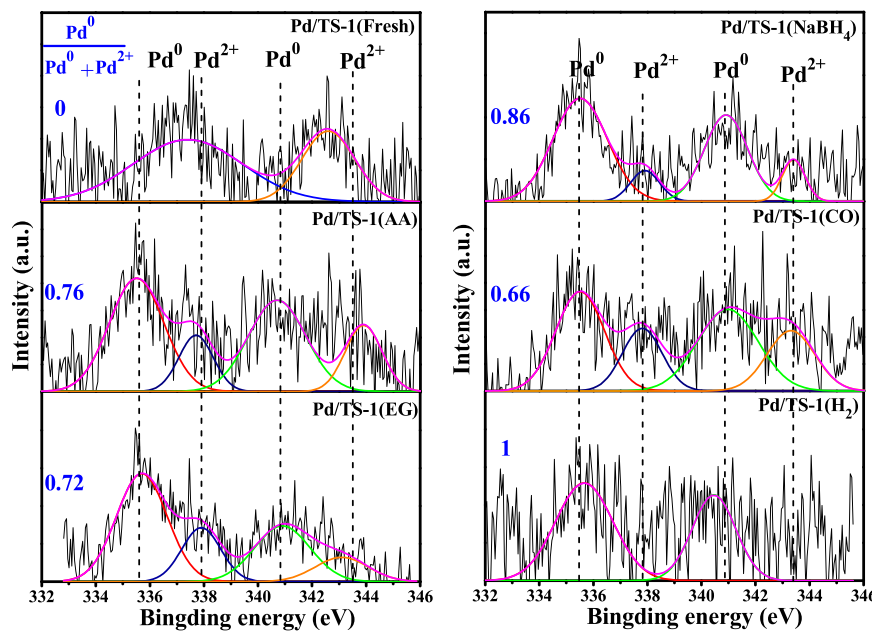


Fig. 5. Pd 3d XPS of Pd/TS-1 pretreated in different reduction atmosphere.

fitting method. According to the previous research, the peaks at BE = 335.5 and 340.8 eV were assigned to the metallic Pd⁰, the other ones at BE = 337.8 and 343.1 eV were attributed to the surface Pd²⁺ species [35]. As for the Pd/TS-1(Fresh) sample calcined in air, Pd mainly exists in the oxidation state (Pd²⁺); while for the sample pretreated in H₂, Pd mostly exists in the metallic state (Pd⁰) on the surface of Pd/TS-1 (H₂). However, palladium coexists as Pd⁰ and Pd²⁺ statuses on the surface of Pd/TS-1(CO), Pd/TS-1(AA), Pd/TS-1(EG) and Pd/TS-1 (NaBH₄). In addition, the ratio of Pd⁰/(Pd⁰+Pd²⁺) on the surfaces of four sample decreased in an order of 0.86 for Pd/TS-1(NaBH₄) > 0.76 for Pd/TS-1(AA) > 0.72 for Pd/TS-1(EG) > 0.66 for Pd/TS-1(CO). Apparently, the Pd⁰/(Pd⁰+Pd²⁺) molar ratio of Pd/TS-1(NaBH₄) was essentially higher than those of other samples, apart from Pd/TS-1(H₂), indicating an outstanding redox properties of the former which promotes the Pd²⁺ → Pd⁰ transfer under an essentially reductive atmosphere due to an easy reduction of NaBH₄ at room temperature. Moreover, it was literature confirmed that a higher Pd⁰/(Pd⁰+Pd²⁺) molar ratio was an indication of better ability to activate oxygen molecules [36].

DRIFTS with CO as molecular probe (CO-DRIFTS) were carried out to investigate ionic and metallic sites in heterogeneous catalysts. The CO-DRIFTS profiles were illustrated in Fig. 6. It could be observed several peaks at 1610, 1719, 1943, 2045, 2130, 2177, and 2226 cm⁻¹. In general, CO adsorption on bulk and supported Pd has been extensively studied so that CO vibrations can now be almost unambiguously assigned. According to the literature report [37], the bands above 2045 cm⁻¹ were assigned to high valence of Pd interacting with CO, while the bands below this wavenumber were assigned to metallic Pd interacting with CO. In short, the ν_{CO} frequencies for CO on Pd are normally assigned as follows: Pd³⁺-CO, 2226 cm⁻¹; Pd²⁺-CO, 2177 cm⁻¹; Pd⁺-CO, 2130 cm⁻¹; Pd⁰-CO (atop), 2045 cm⁻¹; Pd₂⁰-CO (bridging), 1943 cm⁻¹; and Pd₃⁰-CO (3-fold hollow), 1719 and 1610 cm⁻¹ [38,39]. In addition, based on the literature assignment, the absorption peaks at 2045 cm⁻¹, 2130 cm⁻¹ and 2177 cm⁻¹ can also be attributed to an interaction between the Lewis acid site on TS-1 and CO [40,41]. And acidic sites in the Pd/TS-1 samples are perhaps beneficial to the activation of HCHO reactant and promote the removal of HCHO [42]. One could observe that Pd existed in the high valence state on Pd/TS-1(Fresh). It is also well-known that palladium oxides could be reduced by CO, even at subambient. Therefore, Pd⁰-CO and Pd₃⁰-CO

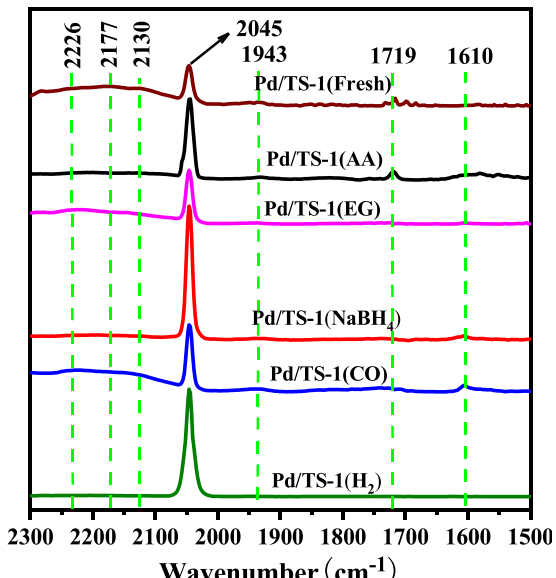


Fig. 6. CO-DRIFTS of Pd/TS-1(Fresh), Pd/TS-1(AA), Pd/TS-1(EG), Pd/TS-1 (NaBH₄), Pd/TS-1(CO), and Pd/TS-1(H₂).

were detectable on Pd/TS-1(Fresh). However, high valence of Pd on the other reduced samples was markedly decreased. Besides, Pd₂⁰-CO (bridging) and Pd₃⁰-CO (3-fold hollow) were also reduced, suggesting that reduction treatment could effectively reduce the agglomeration of Pd nanoparticles. What's more, active component Pd mainly existed in the linear-adsorption metallic state (Pd⁰-CO) especially on Pd/TS-1(H₂) and Pd/TS-1(NaBH₄). According to the literature [43], metallic Pd⁰ is the active center for formaldehyde oxidation. It could be inferred that there were more active sites on these two reduced catalysts.

In order to further confirm the above point of view, CO was also selected as the probe molecule, and CO chemisorption experiments were conducted to investigate the dispersion (D_{Pd}) of Pd nanoparticles, and the results were listed in Table 1. When the sample was pretreated with air, Pd dispersion was only 11.3% on Pd/TS-1(Fresh). After reduction treatment, Pd dispersion was significantly improved with a value of

16.9%, 15.8%, 24.7%, 14.7% and 18.6% for Pd/TS-1(AA), Pd/TS-1(EG), Pd/TS-1(NaBH₄), Pd/TS-1(CO) and Pd/TS-1(H₂), respectively. As one can see, the Pd dispersion was the highest after NaBH₄ reduction, which is consistent with the results of CO-DRIFTS and HRTEM.

3.4. Catalytic performance

Fig. 7 shows the catalytic activity of HCHO oxidation over the as-prepared samples. Obviously, the conversion of HCHO on Pd/TS-1(Fresh) was only about 5%, when the reaction temperature range is 25–100 °C. This indicated that Pd mainly existed in an oxidation state on Pd/TS-1(Fresh) and the ability of activating oxygen was weak on Pd²⁺ species. As for the samples reduced in liquid or gas phase, the conversion of HCHO was more or less improved. At an usually ambient temperature of 25 °C, the HCHO conversion decreases in an order of Pd/TS-1(NaBH₄) > Pd/TS-1(H₂) > Pd/TS-1(AA) > Pd/TS-1(EG) > Pd/TS-1(CO). It is obvious that the Pd/TS-1(NaBH₄) sample could completely remove HCHO even at room temperature.

In addition, Fig. 8 shows the Arrhenius diagram of HCHO oxidation on Pd/TS-1 samples obtained by different pretreatment methods. It has been reported in the literature that the reaction order for VOCs oxidation is close to 1, and the reaction order for oxygen is 0 under the condition of sufficient oxygen [44]. Therefore, it is acceptable that HCHO oxidation reaction follows a first-order reaction kinetic. The apparent activation energies (E_a) were calculated through the fitted slopes. The E_a of reaction occurring over Pd/TS-1(Fresh), Pd/TS-1(AA), Pd/TS-1(EG), Pd/TS-1(NaBH₄), Pd/TS-1(CO) and Pd/TS-1(H₂) were 105.9 kJ/mol, 48.8 kJ/mol, 65.5 kJ/mol, 26.4 kJ/mol, 69.0 kJ/mol and 42.2 kJ/mol, respectively. Obviously, the E_a of HCHO oxidation achieving over Pd/TS-1(NaBH₄) was the smallest among the tested samples, indicating that HCHO oxidation is easily to take place on Pd/TS-1(NaBH₄). In order to further reveal the utilization efficiency of Pd atom, the TOFs on the catalysts were calculated based on Pd dispersion. And the results are listed in Table 1. The Pd/TS-1(NaBH₄) accordingly achieved the highest TOF value ($2.5 \times 10^{-2} \text{ s}^{-1}$), much higher than those of the samples treated by other reductive manners.

Furthermore, the influences of space velocities (SV) and relative humidity (RH) on HCHO oxidation were investigated over the best-performing Pd/TS-1(NaBH₄) catalyst. As shown in Fig. S4(a), the HCHO conversion dropped from 100% to 64% and 42% at 25 °C with increasing the SV from 60,000 to 120,000 and 150,000 mL/(g×h), the decreased activity at high SV might be attributed to the limited

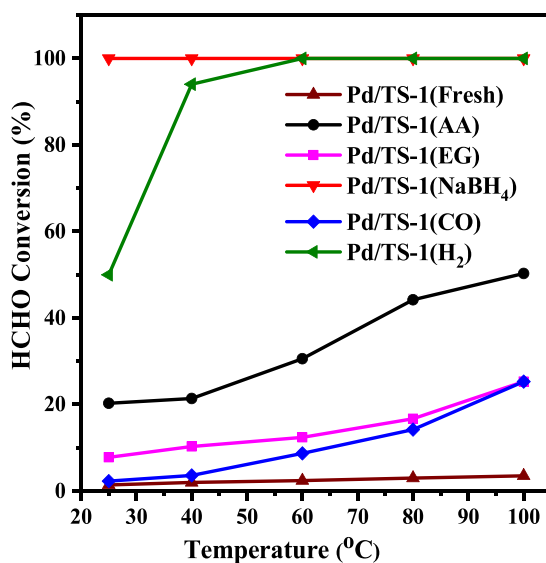


Fig. 7. Activity evaluation of catalytic oxidation of HCHO. Test conditions: 110 ppm HCHO, and SV = 60,000 mL/(g·h).

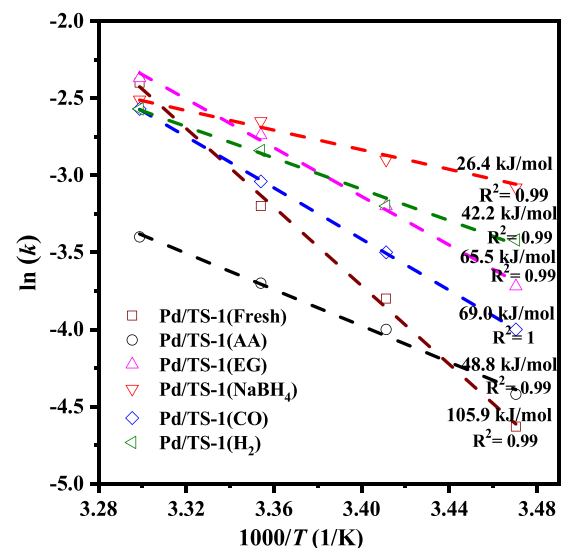


Fig. 8. Arrhenius plots of reaction rate obtained from reaction kinetics over the samples.

contacting time. Water is another important factor to be considered in HCHO oxidation. From Fig. S4(b), one can observe that HCHO conversion dramatically declined to 47% without the addition of water. In contrast, the conversion increased to 100% when the RH reached 35%. The enhanced catalytic activity might be attributed to the formation of -OH groups [45]. However, HCHO conversion dropped to 87% at RH = 75%, indicating excessive quantities of water was hostile for this catalytic oxidation process, which is associated with the competitive adsorption between H₂O and HCHO upon the catalyst.

3.5. Reaction mechanism

The in-situ DRIFTS experiments were conducted on Pd/TS-1(Fresh) and Pd/TS-1(NaBH₄) at room temperature to gain insight into the reaction path of HCHO oxidation and the changes of intermediate species during the reaction. And the results were shown in Fig. 9. The spectra were collected under a certain concentration of HCHO balanced with He at 25 °C. Several characteristic peaks were detected and up to steady state with an extension of time. The bands at 1605–1611, 3514–3588, and 3687 cm⁻¹ were assigned to the -OH group, which gradually declined along with exposure time. While the peaks in the range of 1358–1378, 2860–2894 and 2968–2988 cm⁻¹ were assigned to the stretching vibration of formate (HCOO⁻) [46]. Besides, the bands at 1423–1462 cm⁻¹ were assigned to stretch vibration of dioxymethylene (DOM, CH₂O₂) species, which derived from HCHO interacted with surface active oxygen [47]. The peaks at 1196–1214 cm⁻¹ were attributed to stretch vibration of carbonate (CO₃²⁻) [48], while the band at 1716 cm⁻¹ was assigned to stretch vibration of CO [49]. For the two Pd/TS-1(Fresh) and Pd/TS-1(NaBH₄) samples, a negative absorption peak of -OH group appeared in the short time at the beginning of the reaction, indicating that the reaction began to consume hydroxyl groups. As an active species, -OH can change the reaction pathway of HCHO oxidation. It promotes successive transformation of formate into CO₂ and H₂O [50]. With increasing reaction time, the intensity of DOM and formate gradually increased and reached the maximum. Comparing the two samples, it was found that the accumulation amount of DOM on the Pd/TS-1(Fresh) catalyst was higher than those on Pd/TS-1(NaBH₄), indicating that the DOM could not be rather effectively oxidized on the Pd/TS-1(Fresh) catalyst, which is consistent with the amount of CO. Therefore, the intensity of formate was essentially low on the Pd/TS-1(Fresh) sample. In addition, one could find that the accumulation amount of carbonate on the Pd/TS-1(Fresh) catalyst was higher than

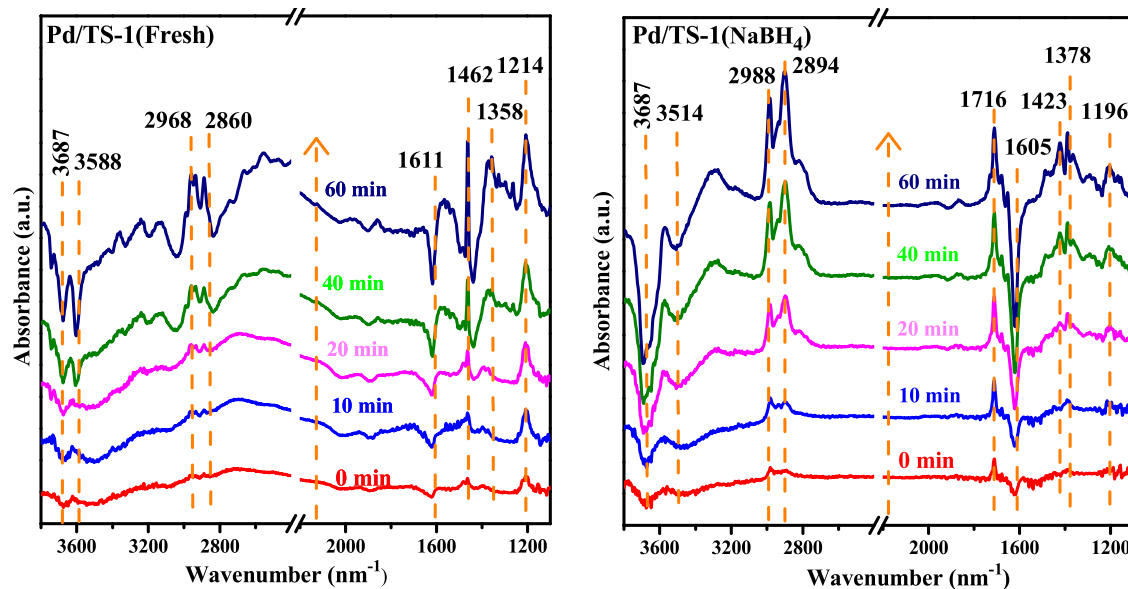


Fig. 9. Time-dependent DRIFTS of the Pd/TS-1(Fresh) and Pd/TS-1(NaBH₄) catalysts under the flow of HCHO/N₂.

those on Pd/TS-1(NaBH₄), suggesting that reduction pretreatment could inhibit the formation of undesirable by-products. The corresponding mechanism is proposed as follows: HCHO was firstly adsorbed on the catalyst surface, and then was oxidized into DOM, HCOOH, and formate species by the surface active oxygens. The main intermediate species directly decomposed into CO adspecies and H₂O, and the adsorbed CO finally converted into CO₂. A small part of the intermediate species (HCOO⁻) reacts with -OH to form CO₂ and H₂O. It is speculated that Pd/TS-1 reduced by NaBH₄ could provide more reactive oxygen species, thus promote the further conversion of formaldehyde and intermediate into final products.

3.6. Discussion

It is generally recognized that the oxidation or reduction pretreatment of the catalyst is a crucial process as for the catalytic oxidation of HCHO. However, the previous studies commonly focus on the effect on chemical state of active component, but ignored the influence on dispersion of noble metals and activation of oxygen species. Herein, the gas-phase reduction at high temperatures and liquid-phase reduction under mild conditions were adopted to pretreat the Pd/TS-1 sample. From the results of XRD and BET, the crystal structure and physical parameters of the samples were marginally changed after reduction treatment, exhibiting the ideal stability of ZSM-5 zeolite framework. However, combining the characterization of HRTEM with CO chemisorption, highly dispersed and small size Pd cluster were obtained on the reduced samples, especially on the sample reduced by NaBH₄. That is to say, the Pd nanoparticles could be uniformly dispersed on the surface of TS-1 after undergoing reductive treatment.

Hereafter, the model structures of Pd nanoparticles containing different number of atoms were built based on the size of Pd according to the present result of HRTEM (Fig. 1). Fig. 10 presents the energy required for the oxygen adsorption, from which the energy for oxygen adsorption followed the increasing order of ΔE_{ads} (Pd₁₁₂) > ΔE_{ads} (Pd₆₄). That was to say, the oxygens are superiorly adsorbed on the Pd particles with less atom numbers; namely, small Pd size are beneficial for O₂ adsorption and further activation.

Furthermore, the catalytic activity and apparent activation energies (E_a) were investigated on the untreated and reduced samples. It was found that the conversion of HCHO followed in an order of Pd/TS-1(NaBH₄) > Pd/TS-1(H₂) > Pd/TS-1(AA) > Pd/TS-1(EG) > Pd/TS-1(CO), and Pd/TS-1(NaBH₄) possessed the small activation energy and high

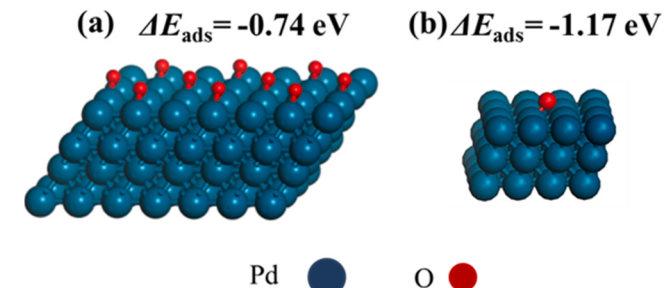


Fig. 10. Model structures of O atom adsorbed on Pd clusters with different size: (a) Pd/TS-1(Fresh) and (b) Pd/TS-1(NaBH₄).

TOF value. In order to reveal the reason, the reducibility of different reducing agents was calculated by ΔG based on the reaction with oxygen. According to the equation $\Delta G = \Delta H - T\Delta S$, the absolute value of ΔG increased in a sequence of Pd/TS-1(NaBH₄) (-213.4 kJ/mol) < Pd/TS-1(H₂) (-203.6 kJ/mol) < Pd/TS-1(CO) (-201.7 kJ/mol) < Pd/TS-1(AA) (118.7 kJ/mol) < Pd/TS-1(EG) (110.2 kJ/mol), fulfilled well with their activity orders. Hence, the reducing pretreatment is thought to be effective manner to well utilize the noble metal and improve the combustion behaviors.

4. Conclusions

The Pd/TS-1 catalyst was pretreated with different reducing gases (H₂, CO) and liquid phase reducing agents (AA, EG, NaBH₄). The results showed that the reduction pretreatment can significantly reduce the size of Pd nanoparticles and improve the Pd dispersion. Besides, the size of Pd nanoparticles was dependent on the way of reduction treatment. In general, the Pd nanoparticles obtained by liquid-phase reduction were more uniform than those by gas-phase reduction at relatively high temperature. And the small size of Pd nanoparticles with 5.1 nm was obtained by using the NaBH₄. Therefore, compared with the Pd/TS-1(Fresh) sample calcined in air, the activity of the reduced samples for catalytic oxidation of HCHO was improved, and the Pd/TS-1(NaBH₄) sample could remove HCHO completely at room temperature. The reduced samples had good low-temperature reducibility and could reduce the aggregation of Pd nanoparticles. Moreover, the size diminution of Pd nanoparticles verified by HRTEM was associated with ideal

redox properties, as evidenced by H₂-TPR. The mechanism study confirmed that the metallic Pd in Pd/TS-1 sample was the active center. Compared with the high valence of Pd²⁺, the metallic Pd was conducive to activate oxygens, transfer intermediate, and inhibit carbonate deposition.

CRediT authorship contribution statement

Zhaoying Di: Writing – review & editing, Data curation, Formal analysis, Software. **Hongxia Chen:** Resources, Writing – original draft preparation, Validation. **Runduo Zhang:** Writing – review & editing, Supervision, Funding acquisition. **Hao Wang:** Software, Validation. **Jingbo Jia:** Project administration, Methodology. **Ying Wei:** Investigation, Visualization.

Declaration of Competing Interest

The authors declare that they have no known competing financial interests or personal relationships that could have appeared to influence the work reported in this paper.

Acknowledgments

The authors thank the National Natural Science Foundation of China (Nos. 22176010, 21976012 and U1862102) and the Fundamental Research Funds for the Central Universities (XK1802-1, JD2117) for the financial support.

Appendix A. Supporting information

Supplementary data associated with this article can be found in the online version at [doi:10.1016/j.apcatb.2021.120843](https://doi.org/10.1016/j.apcatb.2021.120843).

References

- K. Vellingiri, K. Vikrant, V. Kumar, K.H. Kim, Advances in thermocatalytic and photocatalytic techniques for the room/low temperature oxidative removal of formaldehyde in air, *Chem. Eng. J.* 399 (2020), 125759.
- Y. Wan, X. Fan, T. Zhu, Removal of low-concentration formaldehyde in air by DC corona discharge plasma, *Chem. Eng. J.* 171 (2011) 314–319.
- J. Ye, M. Zhou, Y. Le, B. Cheng, J. Yu, Three-dimensional carbon foam supported MnO₂/Pt for rapid capture and catalytic oxidation of formaldehyde at room temperature, *Appl. Catal. B: Environ.* 267 (2020), 118689.
- X. Sun, J. Lin, Y. Wang, L. Li, X. Pan, Y. Su, X. Wang, Catalytically active Ir⁰ species supported on Al₂O₃ for complete oxidation of formaldehyde at ambient temperature, *Appl. Catal. B: Environ.* 268 (2020), 118741.
- Y. Li, C. Wang, C. Zhang, H. He, Formaldehyde oxidation on Pd/TiO₂ catalysts at room temperature: the effects of surface oxygen vacancies, *Top. Catal.* 63 (2020) 810–816.
- G. Huang, Z. Yan, S. Liu, T. Luo, L. An, Z. Xu, Bimetallic nickel molybdate supported Pt catalyst for efficient removal of formaldehyde at low temperature, *J. Environ. Sci.* 87 (2020) 173–183.
- B. Chen, X. Zhu, Y. Wang, L. Yu, J. Lu, C. Shi, Nano-sized gold particles dispersed on HZSM-5 and SiO₂ substrates for catalytic oxidation of HCHO, *Catal. Today* 281 (2017) 512–519.
- J. Zhang, Y. Li, L. Wang, C. Zhang, H. He, Catalytic oxidation of formaldehyde over manganese oxides with different crystal structures, *Catal. Sci. Technol.* 5 (2015) 2305–2313.
- B. Bai, H. Arandiyan, J. Li, Comparison of the performance for oxidation of formaldehyde on nano-Co₃O₄, 2D-Co₃O₄, and 3D-Co₃O₄ catalysts, *Appl. Catal. B: Environ.* 142–143 (2013) 677–683.
- Y. Huang, B. Long, M. Tang, Z. Rui, M.S. Balogun, Y. Tong, H. Ji, Bifunctional catalytic material: an ultrastable and high-performance surface defect CeO₂ nanosheets for formaldehyde thermal oxidation and photocatalytic oxidation, *Appl. Catal. B: Environ.* 181 (2016) 779–787.
- S.B. Shin, D.W. Lee, D.W. Lee, D. Chadwick, The effects of impregnation of precious metals on the catalytic activity of titanium silicate (TS-1) in epoxidation of propene using hydrogen peroxide, *J. Mol. Catal. A: Chem.* 423 (2016) 478–488.
- C. Chen, X. Wang, J. Zhang, S. Pan, C. Bian, L. Wang, F. Chen, X. Meng, X. Zheng, X. Gao, F. Xiao, Superior performance in catalytic combustion of toluene over KZSM-5 zeolite supported platinum catalyst, *Catal. Lett.* 144 (2014) 1851–1859.
- L. Zhang, Y. Jiang, B. Chen, C. Shi, Y. Li, C. Wang, S. Han, S. Pan, L. Wang, X. Meng, F. Xiao, Exceptional activity for formaldehyde combustion using siliceous Beta zeolite as a catalyst support, *Catal. Today* 339 (2020) 174–180.
- H. Chen, R. Zhang, H. Wang, W. Bao, Y. Wei, Encapsulating uniform Pd nanoparticles in TS-1 zeolite as efficient catalyst for catalytic abatement of indoor formaldehyde at room temperature, *Appl. Catal. B: Environ.* 278 (2020), 119311.
- S. Huang, C. Zhang, H. He, Effect of pretreatment on Pd/Al₂O₃ catalyst for catalytic oxidation of o-xylene at low temperature, *J. Environ. Sci.* 25 (2013) 1206–1212.
- J. Liu, Y. Chen, H. Wang, M. Yang, Y. Wu, Z. Chen, Effects of atmosphere pretreatment on the catalytic performance of Pd/γ-Al₂O₃ catalyst in benzene degradation II: crystal structure transformation of Pd active species, *Catal. Today* 297 (2017) 211–218.
- R. Lamber, N. Jaeger, G.S. Ekloff, Metal-support interaction in the Pd/SiO₂ system: influence of the support pretreatment, *J. Catal.* 123 (1990) 285–297.
- D. Chen, Z. Qu, Y. Lv, X. Lu, W. Chen, X. Gao, Effect of oxygen pretreatment on the surface catalytic oxidation of HCHO on Ag/MCM-41 catalysts, *J. Mol. Catal. A: Chem.* 404–405 (2015) 98–105.
- H. Chen, Z. Rui, X. Wang, H. Ji, Multifunctional Pt/ZSM-5 catalyst for complete oxidation of gaseous formaldehyde at ambient temperature, *Catal. Today* 258 (2015) 56–63.
- G. Lv, S. Deng, Z. Yi, X. Zhang, F. Wang, H. Li, Y. Zhu, One-pot synthesis of framework W-doped TS-1 zeolite with robust Lewis acidity for effective oxidative desulfurization, *Chem. Commun.* 55 (2019) 4885–4888.
- J.W. Harris, J. Arvay, G. Mitchell, W.N. Delgass, F.H. Ribeiro, Propylene oxide inhibits propylene epoxidation over Au/TS-1, *J. Catal.* 365 (2018) 105–114.
- T. Maillet, C. Solleau, J. Barbier, D. Duprez, Oxidation of carbon monoxide, propane, and methane over a Pd/Al₂O₃ catalyst, Effect of the chemical state of Pd, *Appl. Catal. B: Environ.* 14 (1997) 85–95.
- X. Gao, J. An, J. Gu, L. Li, Y. Li, A green template-assisted synthesis of hierarchical TS-1 with excellent catalytic activity and recyclability for the oxidation of 2,3,6-trimethylphenol, *Microporous Mesoporous Mater.* 239 (2017) 381–389.
- H. Zhu, Z. Qin, W. Shan, W. Shen, J. Wang, Low-temperature oxidation of CO over Pd/CeO₂–TiO₂ catalysts with different pretreatments, *J. Catal.* 233 (2005) 41–50.
- R.B. Khomane, B.D. Kulkarni, A. Paraskar, S.R. Sainkar, Synthesis, characterization and catalytic performance of titanium silicalite-1 prepared in micellar media, *Mater. Chem. Phys.* 76 (2002) 99–103.
- C. Lamberti, S. Bordiga, A. Zecchina, G. Artioli, G. Marra, G. Spano, Ti location in the MFI framework of Ti-silicalite-1: a neutron powder diffraction study, *J. Am. Chem. Soc.* 123 (2001) 2204–2212.
- H. Hosseiniamoli, A. Setiawan, A.A. Adesina, E.M. Kennedy, M. Stockenhuber, The stability of Pd/TS-1 and Pd/silicalite-1 for catalytic oxidation of methane—understanding the role of titanium, *Catal. Sci. Technol.* 10 (2010) 1193–1204.
- W. Xu, T. Zhang, R. Bai, P. Zhang, J. Yu, A one-step rapid synthesis of TS-1 zeolites with highly catalytically active mononuclear TiO₆ species, *J. Mater. Chem. A.* 8 (2020) 9677–9683.
- G. Zou, W. Zhong, L. Mao, Q. Xu, J. Xiao, D. Yin, Z. Xiao, S.R. Kirk, T. Shu, A non-nitric acid method of adipic acid synthesis: organic solvent- and promoter-free oxidation of cyclohexanone with oxygen over hollow-structured Mn/TS-1 catalysts, *Green Chem.* 17 (2015) 1884–1892.
- S. Bhogeswararao, D. Srinivas, Catalytic conversion of furfural to industrial chemicals over supported Pt and Pd catalysts, *J. Catal.* 327 (2015) 65–77.
- M. Xiong, Z. Gao, Y. Qin, Spillover in heterogeneous catalysis: new insights and opportunities, *ACS Catal.* 11 (2011) 3159–3172.
- C.I. Contescu, C.M. Brown, Y. Liu, V.V. Bhat, N.C. Gallego, Detection of hydrogen spillover in palladium-modified activated carbon fibers during hydrogen adsorption, *J. Phys. Chem. C* 113 (2009) 5886–5890.
- S. Sohrabi, R.K. Abasabadi, A.A. Khodadadi, Y. Mortazavi, A. Hoseinzadeh, In-situ one-step deposition of highly dispersed palladium nanoparticles into zirconium metal–organic framework for selective hydrogenation of furfural, *Mol. Catal.* 514 (2021), 111859.
- Y. Zhang, Y. Cai, Y. Guo, H. Wang, L. Wang, Y. Lou, Y. Guo, G. Lu, Y. Wang, The effects of the Pd chemical state on the activity of Pd/Al₂O₃ catalysts in CO oxidation, *Catal. Sci. Technol.* 4 (2014) 3973–3980.
- N. Xiang, Y. Hou, X. Han, Y. Li, Y. Guo, Y. Liu, Z. Huang, Promoting effect and mechanism of alkali Na on Pd/SBA-15 for room temperature formaldehyde catalytic oxidation, *ChemCatChem* 11 (2019) 5098–5107.
- C. Zhang, Y. Li, Y. Wang, H. He, Sodium-promoted Pd/TiO₂ for catalytic oxidation of formaldehyde at ambient temperature, *Environ. Sci. Technol.* 48 (2014) 5816–5822.
- P. Kast, M. Friedrich, D. Teschner, F. Girsdsies, T. Lunkenbein, R.N. Alnoncourt, M. Behrens, R. Schlägl, CO oxidation as a test reaction for strong metal-support interaction in nanostructured Pd/FeO_x powder catalysts, *Appl. Catal. A: Gen.* 502 (2015) 8–17.
- Y. Zheng, L. Kovarik, M.H. Engelhard, Y. Wang, Y. Wang, F. Gao, J. Szanyi, Low-temperature Pd/zeolite passive NO_x adsorbers: structure, performance, and adsorption chemistry, *J. Phys. Chem. C* 121 (2017) 15793–15803.
- I.V. Yudanov, R. Sahnoun, K.M. Neyman, N. Rosch, J. Hoffmann, S. Schauermann, V. Johanek, H. Unterhalt, G. Rupprechter, J. Libuda, H.-J. Freund, CO adsorption on Pd nanoparticles: density functional and vibrational spectroscopy studies, *J. Phys. Chem. B.* 107 (2003) 255–264.
- O.V. Manoilova, J. Dakka, R.A. Sheldon, A.A. Tsyganenko, Infrared study of Ti-containing zeolites using CO as a probe molecule, *Stud. Surf. Sci. Catal.* 94 (1995) 163–170.
- Y. Xin, Z. Zheng, Z. Luo, C. Jiang, S. Gao, Z. Wang, C. Zhao, The influence of pore structures and Lewis acid sites on selective hydrogenolysis of guaiacol to benzene over Ru/TS-1, *Green Energy Environ.* 5 (2021), <https://doi.org/10.1016/j.gee.2020.12.024>.

[42] L. Zhang, L. Chen, Y. Li, Y. Peng, F. Chen, L. Wang, C. Zhang, X. Meng, H. He, F. Xiao, Complete oxidation of formaldehyde at room temperature over an Al-rich Beta zeolite supported platinum catalyst, *Appl. Catal. B: Environ.* 219 (2017) 200–208.

[43] H. Huang, X. Ye, H. Huang, L. Zhang, D.Y.C. Leung, Mechanistic study on formaldehyde removal over Pd/TiO₂ catalysts: oxygen transfer and role of water vapor, *Chem. Eng. J.* 230 (2013) 73–79.

[44] C. Wong, A.Z. Abdullah, S. Bhatia, Catalytic oxidation of butyl acetate over silver-loaded zeolites, *J. Hazard. Mater.* 157 (2008) 480–489.

[45] H. Chen, Z. Rui, X. Wang, H. Ji, Multifunctional Pt/ZSM-5 catalyst for complete oxidation of gaseous formaldehyde at ambient temperature, *Catal. Today* 258 (2015) 56–63.

[46] C. Ma, C. Yang, B. Wang, C. Chen, F. Wang, X. Yao, M. Song, Effects of H₂O on HCHO and CO oxidation at room-temperature catalyzed by MCo₂O₄ (M=Mn, Ce and Cu) materials, *Appl. Catal. B: Environ.* 254 (2019) 76–85.

[47] J. Chen, M. Jiang, W. Xu, J. Chen, Z. Hong, H. Jia, Incorporating Mn cation as anchor to atomically disperse Pt on TiO₂ for low-temperature removal of formaldehyde, *Appl. Catal. B: Environ.* 259 (2019), 118013.

[48] S.S. Kim, K.H. Park, S.C. Hong, A study on HCHO oxidation characteristics at room temperature using a Pt/TiO₂ catalyst, *Appl. Catal. A: Gen.* 398 (2011) 96–103.

[49] X. Hong, J. Chen, Y. Peng, H. Song, C. Wang, J. Li, Deactivation of Pt-Au/TiO₂-CeO₂ catalyst for co-oxidation of HCHO, H₂ and CO at room temperature: degradations of active sites and mutual influence between reactants, *Appl. Catal. A: Gen.* 582 (2019), 117116.

[50] C. Zhang, F. Liu, Y. Zhai, H. Ariga, N. Yi, Y. Liu, K. Asakura, M. Flytzani-Stephanopoulos, H. He, Alkali-Metal-Promoted Pt/TiO₂ opens a more efficient pathway to formaldehyde oxidation at ambient temperatures, *Angew. Chem. Int. Ed.* 51 (2012) 9628–9632.